Growth process and magnetic properties of iron nanoparticles deposited on Si_3N_4/Si(111)-(8 × 8)

Keitaro Eguchi,[1] Yasumasa Takagi,[1,2] Takeshi Nakagawa,[1,2] and Toshihiko Yokoyama[1,2,*]

[1]*Department of Structural Molecular Science, The Graduate University for Advanced Studies (SOKENDAI), Myodaiji-cho, Okazaki 444-8585, Japan*

[2]*Department of Materials Molecular Science, Institute for Molecular Science, Myodaiji-cho, Okazaki 444-8585, Japan*

(Received 14 June 2011; revised manuscript received 2 April 2012; published 14 May 2012)

We investigated the growth process and magnetic properties of iron deposited on Si_3N_4/Si(111)-(8 × 8) and clean Si(111)-(7 × 7) substrates by scanning tunneling microscopy, x-ray magnetic circular dichroism, and the magneto-optical Kerr effect measurements. These experiments reveal that, on clean Si(111)-(7 × 7), 1.6-monolayer (ML) Fe forms iron silicide with a very small spin magnetic moment of $m_{spin} = 0.17\ \mu_B$, whereas 1.6-ML Fe on Si_3N_4/Si(111) has a much larger spin magnetic moment of $m_{spin} = 2.62\ \mu_B$, which is enhanced compared with that of bcc bulk Fe (2.2 μ_B). The Si_3N_4 surface is found to suppress the silicide formation effectively. Because of weak interaction between Fe and Si_3N_4 and possibly the mismatch of the lattice constant, Fe deposited on Si_3N_4/Si(111) grows as nanoparticles that exhibit superparamagnetism. Above 7.5 ML, most of the nanoparticles locate very closely to each other and become ferromagnetic.

DOI: 10.1103/PhysRevB.85.174415 PACS number(s): 75.20.−g, 68.35.bg, 78.20.Ls, 78.70.Dm

I. INTRODUCTION

The magnetic properties of ferromagnetic transition metals on Si substrates have been widely investigated for use in magnetic devices.[1–13] In the latest decade, the field of spintronics has attracted much attention and the study of low-dimensional materials such as thin films and nanoparticles has become very important. However, clean Si surfaces interact strongly with ferromagnetic transition atoms deposited at room temperature, which leads to the formation of transition-metal silicides. Berling *et al.*[6] reported the Fe magnetic moment that depends on the chemical composition of iron silicides, and showed that the Fe magnetic moment decreases from ∼2.2 μ_B (Fe bulk) to 0 μ_B (FeSi) with increasing the Si concentration. On the other hand, Fe-rich silicides as Fe_3Si are ferromagnetic and are interesting because of high spin polarization with a half metallic character at the Fermi level.[14] Experimentally, the spin polarization of Fe_3Si is reported as 42%–45%.[15,16] In cases of low coverage, iron deposited on Si(111)-(7 × 7) at room temperature, however, FeSi and/or $FeSi_2$ are formed at the initial stage of iron silicidation, which strongly depends upon the experimental conditions.[3,4,11] In any case, the Fe magnetic moment is almost lost by forming Si-rich iron silicides.

To avoid the chemical interaction of Si atoms with ferromagnetic metals and to maintain the large magnetic moments of the metal atoms, several methods have been attempted, which are based on the insertion of insulators,[5] semiconductors,[10] and metals[9,11–13] between the ferromagnetic layers and the Si substrate. For instance, 3-monolayer (ML) Fe films grown on Si(111) coated by CaF_2 with 10-nm thickness show superparamagnetism.[5] The substrate CaF_2/Si(111) has, however, not been characterized well from the viewpoint of surface structure. A GaSe film with 2-nm thickness is also reported as a insertion material that suppresses the diffusion of deposited iron atoms into silicon layers, but unfortunately an Fe-Ga alloy is formed at the interface between GaSe and Fe layers.[10] Deposition of 2.5-ML Au on Si(001) has also been tried and is known to suppress the iron silicide formation to some extent, but some iron silicide is still formed due to diffusion of Fe into the Au layers.[13] It is thus important to find out a modified Si surface, the surface structure of which is well characterized and effectively avoids the formation of silicides to retain the magnetic moment of deposited ferromagnetic metals.

Si_3N_4 is one of the best candidates to prevent intermixing silicon with deposited iron because of its thermal stability. An Si_3N_4 film prepared on Si(111) has been extensively studied,[17–31] and it is known that β-Si_3N_4(0001) grows epitaxially on Si(111) by thermal nitridation with N_2 (N_2^+, N^+),[26,27,31] NO,[28,29] and NH_3.[19–22,30] The lattice mismatch between β-Si_3N_4(0001) ($a_{\beta\text{-}Si_3N_4} = 7.61$ Å) (Ref. 32) and 2 × 2 Si(111) ($2a_{Si} = 7.68$ Å) is only about 1%, which ensures the epitaxial growth of β-Si_3N_4/Si(111)-(8 × 8). The electronic structure of Si_3N_4/Si(111) has also been investigated by photoemission spectroscopy.[20,23,24] It is revealed that the surface states of clean Si(111)-(7 × 7) appearing at the binding energy of 0.2–2.0 eV (Refs. 33 and 34) are diminished after the nitridation and instead new features show up at the binding energies of ∼4 eV (N 2p) and 5.5–12.5 eV (N 2p-Si 3p and N 2p-Si 3s hybridized levels).[20,23] The valence bands of the Si_3N_4 film are found to locate at significantly deeper binding energies than those of clean Si(111)-(7 × 7). The Si_3N_4 film is thus expected to be stable enough to avoid the formation of metal silicide after deposition of transition-metal atoms.

In this study, we have investigated the growth process and magnetic properties of iron deposited on well-defined Si_3N_4/Si(111)-(8 × 8) by using scanning tunneling microscopy (STM), the magneto-optical Kerr effect (MOKE), and x-ray magnetic circular dichroism (XMCD).

II. EXPERIMENTS

Si(111) substrates 12 mm × 4 mm in size were cut from a commercial boron-doped Si(111) wafer (8.4–8.9 Ωcm). After ultrasonic cleaning in ethanol, the crystal was mounted on a nonmagnetic sample holder. The sample was degassed in an ultrahigh vacuum (UHV) chamber by direct heating at ∼800 K for 5–12 h. A reconstructed Si(111)-(7 × 7) surface was obtained by repeated flashing at 1200 K. An Si_3N_4/Si(111)-

(8×8) surface was prepared by following a procedure similar to that reported in the literature.[19,20] Thermal nitridation was conducted at 1130 K with ammonia gas [1×10^{-6} Torr, total exposure of 45 L (1 L = 1×10^{-6} Torr s)]. The substrates were subsequently cooled down slowly to room temperature. The sample cleanliness and order were verified by low-energy electron diffraction (LEED), Auger electron spectroscopy, and STM measurements. Fe was deposited on Si(111)-(7×7) and Si_3N_4/Si(111)-(8×8) substrates at room temperature by using a commercial electron bombardment evaporator. The Fe thicknesses were 1–30 ML [1 ML = 1.217×10^{15} atoms/cm^2, which corresponds to the atomic density of bcc Fe(001) plane] and the deposition rate estimated by a quartz crystal oscillator was 0.5–0.9 ML/min.

The *in situ* STM and MOKE measurements were performed in a UHV system consisting of load lock, sample preparation, STM, and MOKE chambers. Each base pressure was 1×10^{-9}, 8×10^{-11}, 5×10^{-11}, and 3×10^{-10} Torr, respectively. The MOKE chamber was equipped with an electromagnet, and the MOKE measurements were carried out for the polar and longitudinal geometries. A 635-nm commercial laser diode was used as a light source, and the light incident angle was set at 45° in both the polar and longitudinal geometries. The STM and MOKE measurements were performed at 298 K, and some MOKE data were also recorded at low temperature using liquid nitrogen.

The *in situ* XMCD measurements were carried out using the bending magnet Beamline 4B of UVSOR-II in the Institute for Molecular Science (IMS). The details of the XMCD measurement system have been reported in the literature.[35,36] The XMCD measurements were performed at 5 K in a UHV chamber with a 7-T superconducting magnet. The circular polarization factor was estimated to be $P_c = 0.60$ from the storage ring parameters, which was verified by the XMCD measurements of a standard sample. The magnetic field of ±5 T was applied to the sample in parallel and antiparallel geometries with respect to the x-ray beam. The x-ray incidence angles with respect to the surface normal were 0° (normal x-ray incidence) and 55° (grazing incidence), and the XMCD spectra were obtained in the total electron yield (TEY) mode.

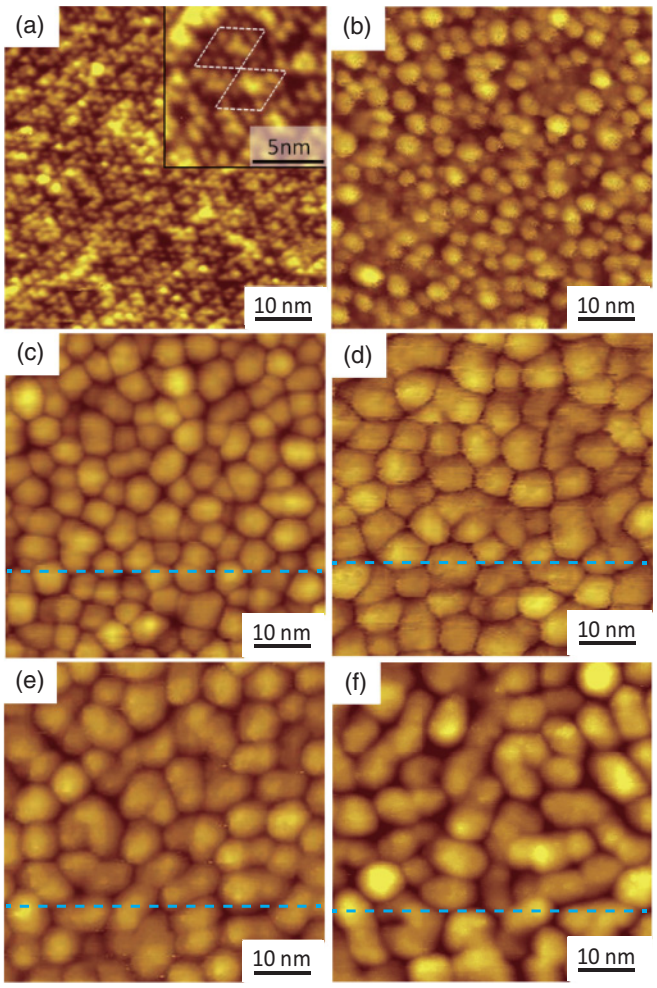

FIG. 1. (Color online) 55×55 nm^2 STM images of (a) Si_3N_4/Si(111)-(8×8) substrate and iron-deposited films with Fe coverages of (b) 1.0 ML, (c) 4.0 ML, (d) 7.5 ML, (e) 10 ML, and (f) 15 ML. The deposition temperature was 298 K. These images were taken at the sample biases of +2.6 V [(a)–(e)] and +0.5 V [(f)], and the tunneling currents of ∼115 pA [(a)–(d)] and ∼160 pA [(e) and (f)]. In panel (a), a magnified image is inserted, in which the white dashed line shows the (8×8) superlattice. The blue dashed lines in panels (c)–(f) represent the line of section views in Fig. 2(b).

III. RESULTS AND DISCUSSION

A. Morphology of Fe on Si_3N_4/Si(111)

STM images of Fe (0–15 ML) deposited on Si_3N_4/Si(111) are shown in Fig. 1. Figure 1(a) shows the STM image of the Si_3N_4/Si(111)-(8×8) substrate surface, and a magnified image with the lattice marked by dashed lines is inserted in the upper-right corner. The STM image of the 1-ML Fe-deposited sample [Fig. 1(b)] shows the formation of Fe nanoparticles. A histogram of the nanoparticle diameters is shown in Fig. 2. For 1.0-ML Fe, the average nanoparticle diameter is 3.3 ± 0.5 nm and more than 90% of the nanoparticles are included in the diameter range of 3.5 ± 1.0 nm, implying that they are uniform in size, although these nanoparticles are not aligned to a certain direction. This result is similar to the previous report by Flammini *et al.*[23] that the growth of Au on Si_3N_4/Si(111) follows the Volmer-Weber mode. Although the chemical composition of the nanoparticles can not be determined by the STM measurements, the present nanoparticles are found to consist essentially of pure Fe from the x-ray absorption spectroscopy (XAS) measurement described in the next section, which demonstrates that the deposited Fe atoms have no chemical bonds with Si or N atoms.

For 4.0- and 7.5-ML Fe [Figs. 1(c) and 1(d)], the nanoparticles form similarly to the case of 1.0-ML Fe. With increasing Fe coverage, the particle size in the lateral direction increases gradually. The mean particle size for 4.0- and 7.5-ML Fe are 5.0 ± 0.9 and 6.9 ± 1.2 nm, respectively. For 7.5-ML Fe, neighboring nanoparticles are located very close to each other, and some particles are apparently connected. For 10-ML Fe, half of nanoparticles are coalesced to the neighboring nanoparticles. Considering the mean particle size of 6.9 ± 1.2 nm for 7.5-ML Fe, the nanoparticles grow up to ∼7 nm in a lateral diameter, which corresponds to the mean

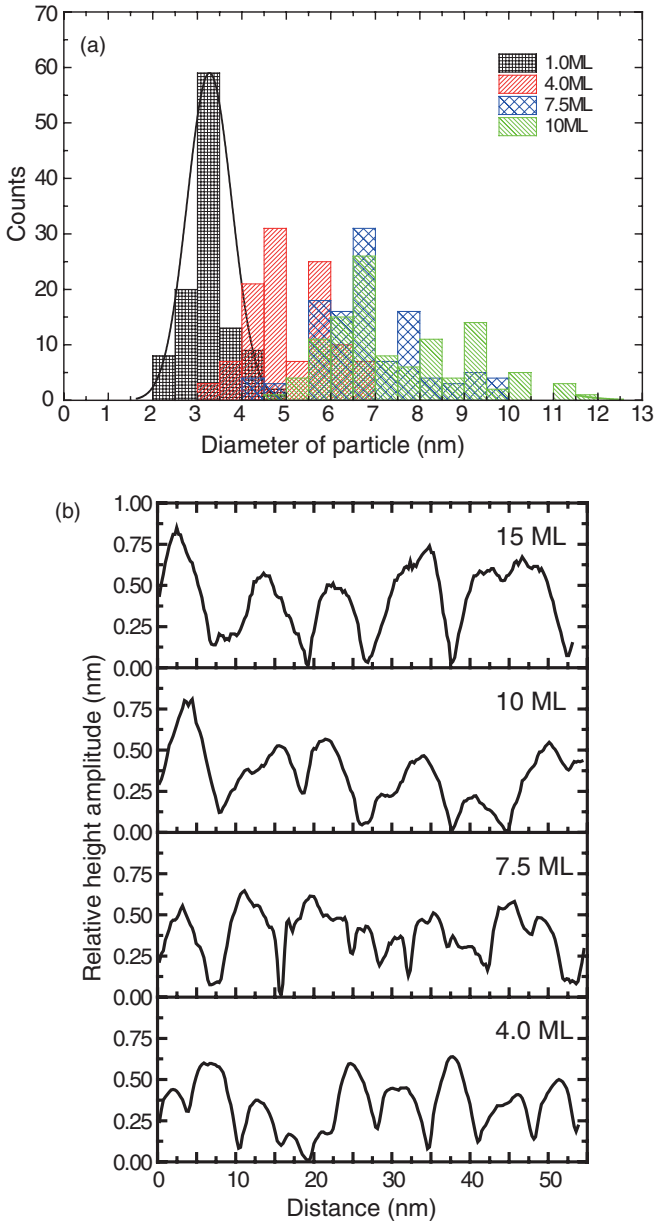

FIG. 2. (Color online) (a) Histograms of the diameters of iron nanoparticles. The Fe coverages are 1.0, 4.0, 7.5, and 10 ML. The solid line is the Gaussian fit. The average diameters of the Fe nanoparticles are 3.3, 5.0, 6.9, and 7.5 nm, respectively. (b) Section views of STM images in Figs. 1(c)–1(f).

distance between the centers of the nearest nanoparticles. For greater than 15 ML, most nanoparticles are connected to each other and tend to form inhomogeneous structures. Thus, it is obvious that the lateral size of the nanoparticles increases with the Fe coverage.

In order to discuss the vertical size of the nanoparticles as a function of Fe coverage, section views of the STM images for 4.0–15 ML [Figs. 1(c)–1(f)] are shown in Fig. 2(b). It is noted that the relative height of nanoparticles in the section views does not correspond to the amount of the Fe coverage because the narrow gap width between the nanoparticles can not be measured precisely due to large curvature of the STM tip. It is thus difficult to discuss the absolute height of the nanoparticles from the substrate surface level from the present STM results. It is, however, found that the relative height of the nanoparticles increases gradually with the Fe coverage. In addition, root mean squares (RMS) of the nanoparticles along the vertical direction estimated from the present STM images are 0.301 nm for 4.0 ML, 0.380 nm for 7.5 ML, 0.384 nm for 10 ML, and 0.694 nm for 15 ML, respectively. It is reasonable that the vertical height of the nanoparticle increases monotonically with the Fe coverage. It is concluded that the iron deposited on the Si_3N_4 surface forms metallic nanoparticles and follows the Volmer-Weber growth mode as in the case of Fe deposited on Au/Si_3N_4 (Ref. 23).

We also performed LEED measurements to investigate the differences of the growth process of the nanoparticle between on the clean Si(111) surface and on the Si_3N_4 surface. The LEED images taken in various thicknesses are shown in Fig. 3. The 7×7 LEED pattern is visible for the clean Si surface [Fig. 3(a)]. When 1.0-ML Fe is deposited on the clean surface [Fig. 3(b)], the 1/7 order spots disappear while the 1×1 fundamental spots remain. This indicates that the deposited Fe atoms react with the reconstructed Si atoms and the 7×7 order structure are destroyed. In addition, broad 1×1 spots emerge almost at the same position as the sharp 1×1 spots originating from the Si substrate. The new broad spots should originate from iron silicides because the CsCl-type FeSi (Refs. 37 and 38) and $FeSi_2$ (Refs. 39–41) are known to grow epitaxially on Si(111). For 2.0-ML Fe deposited on the clean surface [Fig. 3(c)], the sharp 1×1 spots disappear and the only broad 1×1 spots are visible. This means that the iron silicides cover almost the entire surface of the Si(111) substrate. The broad spots subsequently become more intense with trigonal symmetry for 26-ML Fe [Fig. 3(e)], which indicates the growth of an epitaxial film. It is already reported that epitaxial bcc Fe(111) is grown on Si(111) at room temperature at the Fe coverage more than 3.2 (Ref. 42) or 4.5 ML (Ref. 1). It is thus expected that bcc Fe(111) is epitaxially grown on the clean Si surface at 26-ML Fe owing to buffer layers of the iron silicides.

On the contrary, it is obvious that the fractional spots of the 8×8 pattern remain when 1.0-ML Fe is deposited on the Si_3N_4 surface [Fig. 3(g)]. The fractional spots are still visible for 4.0-ML Fe [Fig. 3(h)]. Both the fundamental and fractional spots vanish completely for 7.5-ML Fe [Fig. 3(i)]. This finding means that the Fe atoms deposited on the Si_3N_4 surface form three-dimensional islands without chemical interaction with the Si or N atoms, and the entire Si_3N_4 surface is almost covered by the Fe islands at 7.5-ML Fe. For 26-ML Fe [Fig. 3(j)], there are no apparent spots such as the trigonal broad spots in Fig. 3(e). It is found that Fe deposited on the Si_3N_4 surface does not grow epitaxially in contrast to the case of the clean surface.

In summary, the structures and growth processes of Fe deposited on the clean and Si_3N_4 surfaces are as follows. For Fe/Si(111), the iron silicide clusters are formed at the initial stage,[1,3,43] and subsequently the epitaxial Fe films grow on the iron silicide in thick coverage. Namely, the iron silicide plays a role of buffer layers to form resultantly metallic Fe layers. The growth mode of Fe deposited on the Si_3N_4 is different from that on the clean surface. For Fe/Si_3N_4/Si(111), the Si_3N_4 surface is sufficiently inactive so that pure Fe nanoparticles can be

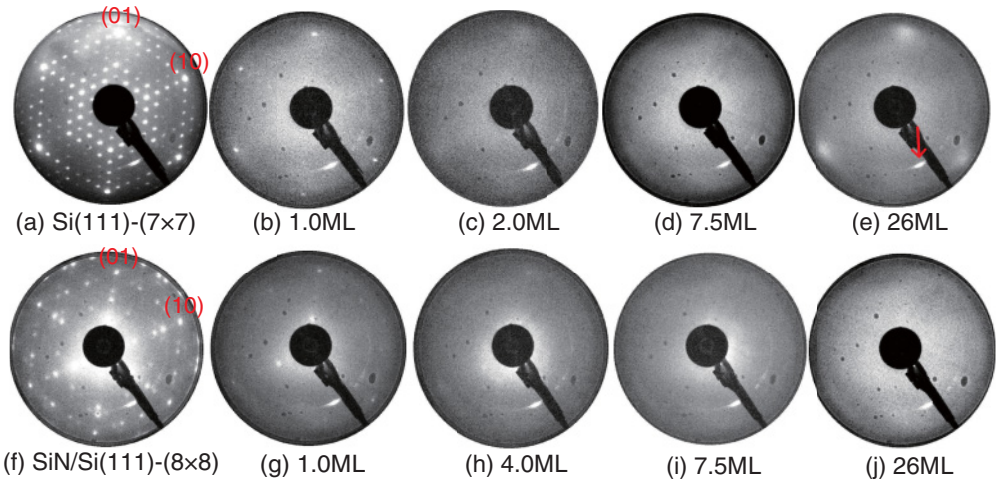

FIG. 3. (Color online) LEED paterns for Fe deposited on the clean surface [(a)–(e)] and the Si_3N_4 surface [(f)–(j)] obtained at room temperature as a function of Fe coverage. The all patterns were measured at 36 eV. Architectural spots as shown in panel (e) by an arrow is observed at the same position in all the images. The spots are caused by the light of filament.

grown without iron silicide formation, and the Fe nanoparticles grow as islands with increasing the Fe coverage. The connected nanoparticles do not grow epitaxially after the nanoparticles are covered with the surface at the Fe coverage of 7.5 ML.

B. Magnetic properties

Figure 4(a) shows the circularly polarized Fe $L_{III,II}$-edge XAS of iron (1.6 ML) on Si(111)-(7 × 7) and Si_3N_4/Si(111)-(8 × 8) recorded at a temperature of 5 K, an external magnetic field of ±5 T, and a x-ray incident angle of 55° (grazing incidence). The spectra were normalized by the edge jumps. The spectra of Fe/Si_3N_4/Si(111) are quite different from those of Fe/Si(111). The previous studies on iron silicide[16,44] and iron nitride[45] have shown that additional peaks are observed at a higher photon energy side of the main peaks. The spectral feature can be used as a fingerprint to confirm whether Fe atoms are bonded to Si and/or N atoms. In the present measurement, a shoulder structure is seen on the high-energy side of the main peak at the Fe L_{III} edge for Fe/Si(111), as in the case of iron silicide. On the contrary, no shoulder structure appears in those of Fe/Si_3N_4/Si(111), indicating that the Fe atom on the Si_3N_4 surface does not interact strongly with the Si or N atoms.

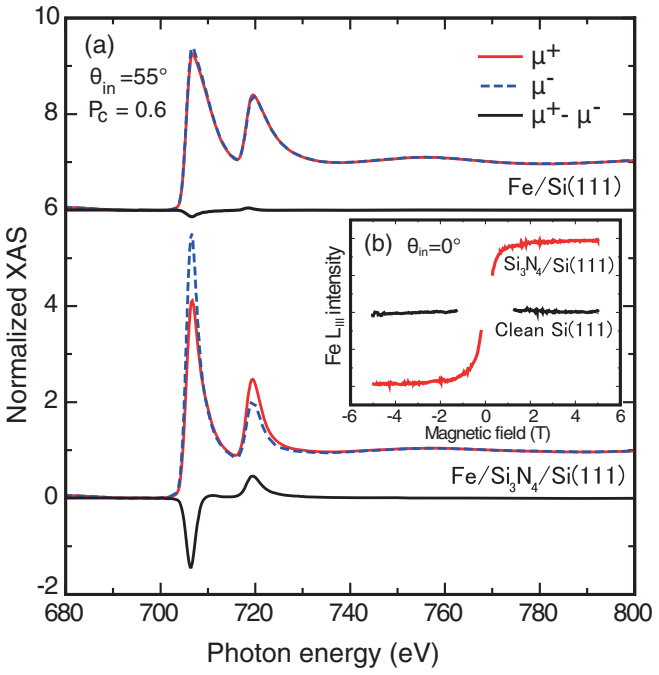

FIG. 4. (Color online) (a) Fe $L_{III,II}$-edge circularly polarized x-ray absorption spectra of 1.6-ML Fe on Si(111)-(7 × 7) (top) and on Si_3N_4/Si(111)-(8 × 8) (bottom) at $\mu_0 H = \pm 5$ T, $T = 5$ K, and the x-ray incidence angle θ_{in} of 55°. (b) Magnetization curves of 1.6-ML Fe on Si(111)-(7 × 7) (black) and Si_3N_4/Si(111)-(8 × 8) (red) at $T = 5$ K, obtained by recording the TEY with the photon energy fixed at the L_{III} peak top of ~707 eV.

The magnetization (M-H) curves were also recorded using the Fe L_{III}-edge peak intensity for each substrate [see Fig. 4(b)], and found that the Fe atoms are not at all magnetized on the clean Si(111) surface. This implies that iron silicides form on clean Si(111). Conversely, the Fe atoms are clearly magnetized on the Si_3N_4 surface, which indicates effective suppression of iron-silicide formation. These results are in good agreement with the results concerning Au deposition on Si_3N_4/Si(111).[23] The study on Au/Si_3N_4/Si(111) showed that the Au atoms do not have chemical bonds with Si at room temperature. Aballe *et al.*[46] further found out that at a temperature higher than 450 °C, the Au atoms on Si_3N_4/Si(111) begin to penetrate the Si_3N_4 layers and to form Au-Si bonds.

The reason why the iron-silicide formation is suppressed at the Fe-Si_3N_4 interface can be interpreted as follows. The binding energies of the surface states of Si(111)-(7 × 7) originating from the adatoms and rest atoms are known to be less than ~1 eV (Ref. 33) or around 0.2, 0.8, and 1.8 eV (Ref. 34) below the Fermi level. The bulk state appears at a deeper binding energy around 2 eV.[47] On the other hand, in the case of Si_3N_4/Si(111)-(8 × 8), no peaks were observed at less than 4 eV in the binding energy,[23,24] and the valence electrons belonging to N 2p and hybridized N 2p-Si 3p and N 2p-Si 3s states are located at 4.0, 7.1, and 11.0 eV,

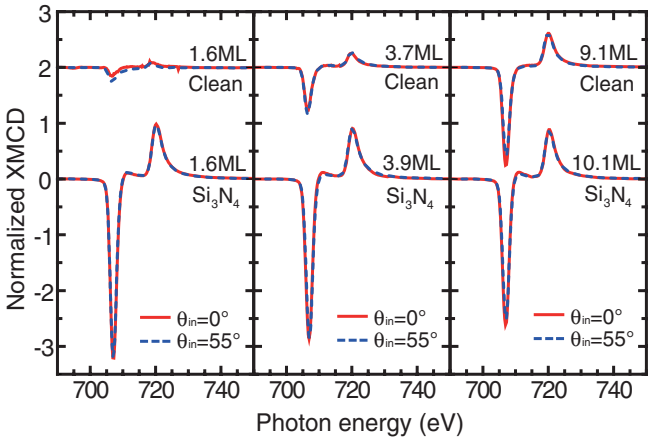

FIG. 5. (Color online) Fe $L_{\mathrm{III,II}}$-edge XMCD of Fe on clean Si(111)-(7 × 7) and Si_3N_4/Si(111)-(8 × 8) at $\mu_0 H = \pm 5$ T, $T = 5$ K, and $\theta_{\mathrm{in}} = 0^\circ$ and 55° in the TEY mode.

respectively.[23] Dufour *et al.*[33] also detected the same three peaks in the energy range of 4–12 eV. Moreover, it has been confirmed that on clean Si(111), the STS (scanning tunneling spectroscopy) peaks assigned to the occupied levels of the Si adatom and the back bond appear at 0.4 and 1.8 eV, respectively, while on Si_3N_4/Si(111)-(8 × 8) the STS peak of the N adatom is observed at ∼4.2 eV.[19] It is thus recognized that iron-silicide formation is effectively suppressed on the Si_3N_4 surface because the energy levels of the valence electrons such as N 2*p*, N 2*p*-Si 3*p*, and N 2*p*-Si 3*s* are too deep to exchange the chemical bonds from Si-N to Si-Fe or N-Fe.

Figure 5 shows the Fe *L*-edge XMCD spectra of Fe on Si(111)-(7 × 7) (1.6, 3.6, and 9.1 ML) and Si_3N_4/Si(111)-(8 × 8) (1.6, 3.9, and 10.1 ML), taken at incident x-ray angles of 0° and 55°, a magnetic field of ±5 T, and a temperature of 5 K. On clean Si(111), almost no XMCD signals can be seen in 1.6-ML Fe and are gradually enhanced with the increase in Fe thickness, although the XMCD signals are still weaker than those of Fe/Si_3N_4/Si(111). On the contrary, strong XMCD signals are found for Si_3N_4/Si(111)-(8 × 8), which are the largest at the lowest Fe coverage (1.6 ML) and are slightly reduced with the Fe coverage.

We have evaluated quantitatively the spin and orbital magnetic moments of the Fe atom in a similar manner to the previous studies.[35,36] We have employed the XMCD sum rules for the orbital (m_{orb}) and effective spin ($m_{\mathrm{spin}}^{\mathrm{eff}}$) magnetic moments.[48,49] The angle-dependent XMCD analysis at saturation magnetization was subsequently performed to eliminate the contribution of the spin dipole moment (m_{T}) and obtain the pure spin magnetic moment (m_{spin}).[50] The *d*-hole number n_d was also obtained by scaling the white-line intensity with the assumption that n_d for 10.1-ML Fe on Si_3N_4/Si(111)-(8 × 8) is the same as that of the bulk ($n_d = 3.40$). The spin dipole moments were found to be negligibly small for all the samples analyzed. The results of the analysis are tabulated in Table I. For Fe on clean Si(111), the spin magnetic moment increases monotonically and the *d*-hole number decreases with increasing the Fe coverage. It is concluded that the Fe atoms near the surface do not form silicides in thicker coverages and are present as metallic iron. A larger *d*-hole number in

TABLE I. Results of the Fe $L_{\mathrm{III,II}}$-edge XMCD analysis for Fe on Si(111)-(7 × 7) and Si_3N_4/Si(111)-(8 × 8). For the orbital magnetic moment m_{orb}, surface parallel (∥) and normal (⊥) components are given separately. The *d*-hole number n_d is also tabulated.

Substrate	Si(111)-(7 × 7)			Si_3N_4/Si(111)-(8 × 8)		
coverage (ML)	1.6	3.7	9.1	1.6	3.9	10.1
$m_{\mathrm{spin}}(\mu_{\mathrm{B}})$	0.17	0.74	1.59	2.62	2.52	2.28
$m_{\mathrm{orb}}^{\parallel}(\mu_{\mathrm{B}})$	0.15	0.05	0.08	0.15	0.17	0.12
$m_{\mathrm{orb}}^{\perp}(\mu_{\mathrm{B}})$	0.00	0.05	0.11	0.18	0.20	0.16
n_d	4.12	3.60	3.40	3.40	3.40	3.40

Fe/Si(111) is also indicative of the silicide formation because of a larger electronegativity of Si than Fe. In contrast to Fe on clean Si(111), the spin magnetic moment of Fe on the Si_3N_4 surface is 2.62 μ_{B} for 1.6 ML and decreases gradually toward the bulk value of 2.2 μ_{B} with increasing the Fe coverage. The Fe atoms on the Si_3N_4 surface do not react with Si and the spin magnetic moment is enhanced due to the size effect. In the 1.6-ML Fe coverage, the spin magnetic moment is about 18% larger than the bulk value. Similarly, the orbital magnetic moments are drastically enhanced compared to the bulk Fe value of 0.085 μ_{B}.[51] We will here emphasize the enhancement of the Fe spin and orbital magnetic moments by suppressing the iron silicide formation.

We also investigated the dependence of the magnetic properties of the iron nanoparticles on the Fe coverage in greater detail by MOKE measurements at 298 K. Although both the polar and longitudinal configurations were attempted, no hysteresis loop was obtained for the polar configuration, implying that the present Fe films have in-plane magnetic easy axes. Typical magnetization curves of Fe/Si(111) and Fe/Si_3N_4/Si(111) are plotted in Figs. 6(a) and 6(b), and the Kerr rotations at saturated magnetization are shown in Fig. 6(c) as a function of the Fe coverage. The numerical values of the Kerr rotation angles were obtained by taking the average of two magnetization curves for each sample. The Kerr rotation angles at saturated magnetization were estimated by extrapolating the magnetization curve in the high magnetic field regions toward the zero magnetic field. In both Fe/Si(111) and Fe/Si_3N_4/Si(111) of Fig. 6(c), the thickness dependence curves show abrupt increase above the critical thicknesses at ∼5 and ∼9 ML, respectively. Below the critical thickness, the system is paramagnetic at room temperature, while it is ferromagnetic above the critical thickness. For the Fe coverage greater than 15 ML, the Kerr rotation of Fe/Si_3N_4/Si(111) is clearly larger than that of Fe/Si(111). This is because a part of the Fe magnetic moment on the clean Si(111) surface is lost due to the formation of iron silicide. The thickness of the dead layer is estimated as ∼2 ML from the present XMCD results and the previous photoelectron spectroscopic results in the Fe/Si(111) system as reported in Ref. 11.

It is, however, interesting that the critical thickness of ferromagnetism is smaller in Fe/Si(111) than in Fe/Si_3N_4/Si(111). In Fe/Si(111), although the magnetically dead layer consisting of iron silicide with ∼2 ML thickness is formed at the initial stage, the Fe layers grow on the iron silicide surface rather than the Fe nanoparticle islands. This causes a smaller

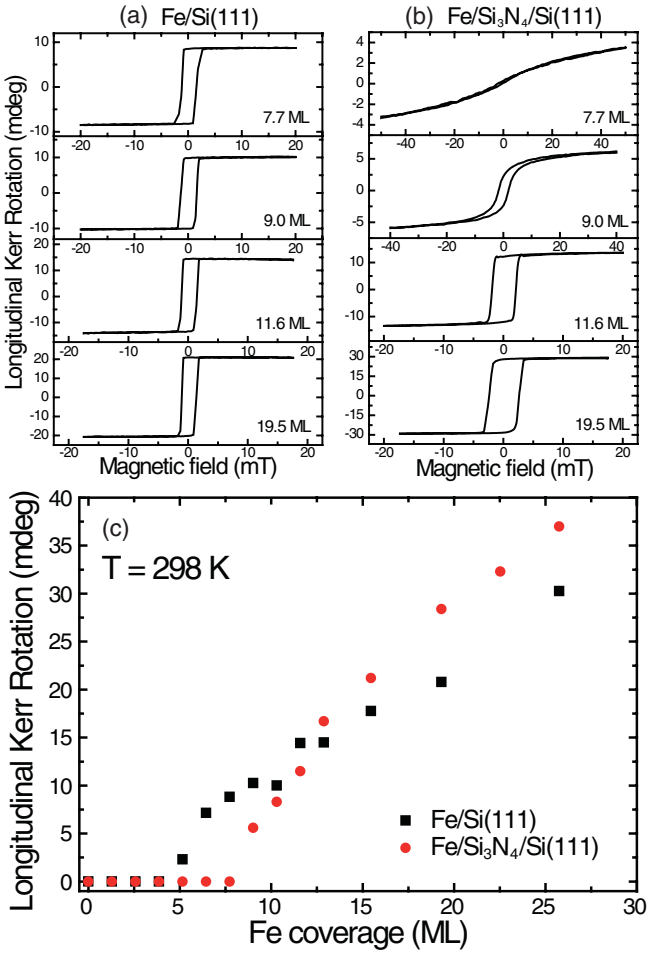

FIG. 6. (Color online) Magnetization curves of (a) Fe/Si(111) and (b) $Fe/Si_3N_4/Si(111)$ at 298 K recorded by the longitudinal MOKE measurements, and (c) the longitudinal Kerr rotation angle as a function of Fe coverage for Fe/Si(111) (black squares) and $Fe/Si_3N_4/Si(111)$ (red circles).

critical thickness of the ferromagnetism in Fe/Si(111) than in $Fe/Si_3N_4/Si(111)$. To understand the behavior in more detail, we measured the temperature dependence of the Kerr effect of 7.7-ML Fe on $Si_3N_4/Si(111)$ down to 125 K. We found no hysteresis loop in the magnetization curve at 298 K but a small remanence at 125 K, as shown in Fig. 7(a). The magnetic susceptibility and its inverse at $\mu_0 H = 0$ are plotted

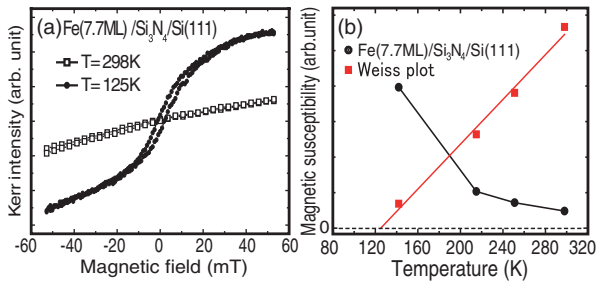

FIG. 7. (Color online) (a) Magnetization curves of Fe(7.7 ML)/$Si_3N_4/Si(111)$ at 298 and 125 K, recorded in the longitudinal MOKE measurements. (b) Temperature dependence of the magnetic susceptibility (black circles) and the Weiss plot (red squares).

in Fig. 7(b). The Weiss temperature is estimated to be ~125 K. It is concluded that the transition from a paramagnetic to ferromagnetic phase occurs at around 125 K.

In order to understand the origin of the magnetic phase transition, let us first consider whether each Fe nanoparticle is magnetized at room temperature (superparamagnetic) or not. From the present STM observation in Figs. 1(d) and 2(a), the average diameter of the Fe nanoparticle in 7.7-ML Fe is 7 nm. Assuming the nominal thickness of 7.7 ML from the quartz thickness monitor, the number of Fe atoms N in a nanoparticle is estimated to be $\sim 3.6 \times 10^3$, independent of the shape of the nanoparticle. The Curie temperatures of the Fe nanoparticles have been reported by several previous works. Billas *et al.*[52] obtained the magnetic moments of Fe clusters with 50–600 Fe atoms that are around 3.0–1.8 μ_B at 300 K. Evans *et al.*[53] theoretically showed that the Curie temperature for the 432-atom Fe particle is only slightly lower than the bulk value (sufficiently higher than 298 K). Since the present nanoparticle is much larger than those of the previous works, it is recognized that the present Fe nanoparticles on $Si_3N_4/Si(111)$ is superparamagnetic at 298 K.

Next, we will discuss the origin of the remanence in the Fe nanoparticles at low temperature. There should be two possibilities for the remanence at low temperature: magnetic dipole-dipole interaction between the nanoparticles or high blocking temperature of the nanoparticle. The magnetic dipole-dipole interaction E_{dd} is expressed based on the classical theory as

$$E_{dd} \sim \frac{\mu_0}{4\pi} \frac{\mu^2}{r_{pp}^3}, \tag{1}$$

where μ is the magnetic moment of the nanoparticle and r_{pp} is the distance between the centers of the nanoparticles. The ordering temperature T_{dd} of the system is given by

$$T_{dd} \sim \frac{\mu_0}{4\pi} \frac{\mu^2}{k_B r_{pp}^3}. \tag{2}$$

In the present 7.7-ML Fe case, with the assumptions of $r_{pp} = 7.0$ nm and $\mu = N m_s \sim 8.3 \times 10^3$ μ_B, the ordering temperature T_{dd} is estimated to be ~125 K, which matches well the Weiss temperature given by the MOKE.

On the other hand, the superparamagnetic blocking temperature T_b of the Fe nanoparticle can be estimated as

$$T_b \sim \frac{KV}{k_B \ln(\tau_m/\tau_0)}, \tag{3}$$

where τ_m is the relaxation time (~100 s), τ_0 the attempt time ($\sim 10^{-11}$ s), V the volume of the nanoparticle, K the magnetic anisotropy constant, and k_B the Boltzmann constant. Several previous experimental reports show the blocking temperatures of 1–54 K for Fe nanoparticles and clusters.[54–58] For the present nanoparticles, assuming $K = 4.5 \times 10^4$ J/m^3 (the bulk Fe value), the blocking temperature T_b is estimated to be only ~5 K, which is much lower than the present observation of ~125 K. It is thus concluded that the magnetic dipole-dipole interaction plays a dominant role on the ferromagnetic behavior of the Fe nanoparticles at low temperature.

In the case of very low Fe coverage as 1-ML Fe, the effect of the magnetic dipole-dipole interaction is neglected because the distance between the nanoparticles r_{pp} is obviously too

large. With the assumptions of the average particle diameter of 3.3 nm, a height of 0.4 nm (the number of atoms in a nanoparticle N of ∼190), the particle distance r_{pp} of 4.2 nm, and the magnetic moment of 2.6 μ_B from the STM and XMCD results, the magnetic dipole-dipole interaction for 1-ML Fe is given as only ∼2 K. In this situation, the blocking temperature T_b is estimated also to be ∼0.4 K by using the bulk magnetic anisotropy constant, although the magnetic anisotropy should be larger than the bulk value. The Fe nanoparticles in small coverages such as 1 ML are thus superparamagnetic and show no remanence, which is consistent with the XMCD results in Fig. 4(b).

IV. CONCLUSIONS

We investigated the morphology and magnetic properties of Fe nanoparticles grown on a Si_3N_4/Si(111)-(8 × 8) substrate by STM, MOKE, and XMCD measurements. The deposited Fe does not form iron silicide, which is an essentially different behavior from Fe on clean Si(111). The Si_3N_4 film works excellently as a well-ordered inert substrate to avoid the formation of nonmagnetic silicides. Because of weak interactions between the transition metals and the Si_3N_4 substrate and also possibly of mismatch of the lattice constant, the deposited Fe grows as nanoparticles. The 1.6-ML Fe exhibits a spin magnetic moment of 2.62 μ_B, which is significantly enhanced compared with that of bulk bcc Fe due to the size effect. The Fe nanoparticles show superparamagnetism and, above ∼7.5 ML, the nanoparticles locate closely to each other and become ferromagnetic at low temperature due to the magnetic dipole-dipole interaction between the nanoparticles.

ACKNOWLEDGMENTS

The authors gratefully acknowledge the UVSOR-II staff at the IMS, especially E. Shigemasa and H. Zen, for their technical help during the XMCD measurements. We also wish to thank T. Yano for his technical support in preparing the sample holders, and X. D. Ma for fruitful discussion. This study was supported by a Grant-in-Aid for Scientific Research (A) (Grant No. 22241029) of the Japan Society for the Promotion of Science (JSPS).

*yokoyama@ims.ac.jp

[1] K. Kataoka, K. Hattori, Y. Miyatake, and H. Daimon, Phys. Rev. B **74**, 155406 (2006).
[2] Y. Ufuktepe and M. Onellion, Solid State Commun. **76**, 191 (1990).
[3] J. Alvarez, A. L. Vazquez de Parga, J. J. Hinarejos, J. de la Figuera, E. G. Michel, C. Ocal, and R. Miranda, Phys. Rev. B **47**, 16048 (1993).
[4] M. Matsumoto, K. Sugie, T. Kawaguchi, K. Fukutani, and T. Okano, Jpn. J. Appl. Phys. **45**, 2390 (2006).
[5] K. R. Heim, G. G. Hembree, and M. R. Scheinfein, J. Appl. Phys. **76**, 8105 (1994).
[6] D. Berling, G. Gewinner, M. C. Hanf, K. Hricovini, S. Hong, B. Loegel, A. Mehdaoui, C. Pirri, M. H. Tuilier, and P. Wetzel, J. Magn. Magn. Mater. **191**, 331 (1999).
[7] A. A. Alekseev, I. A. Kuyanov, and A. V. Zotov, Zh. Tekh. Fiz. **79**, 1 (2009) [Tech. Phys. **54**, 1561 (2009)].
[8] G. Garreau, S. Hajjar, J. L. Bubendorff, C. Pirri, D. Berling, A. Mehdaoui, R. Stephan, P. Wetzel, S. Zabrocki, G. Gewinner, S. Boukari, and E. Beaurepaire, Phys. Rev. B **71**, 094430 (2005).
[9] P. Castrucci, R. Gunnella, R. Bernardini, M. De Crescenzi, L. Ferrari, C. Crotti, C. Comiccioli, C. Ottaviani, G. Gubbiotti, and G. Carlotti, Surf. Sci. **476**, 43 (2001).
[10] M. Eddrief, Y. Wang, V. H. Etgens, D. H. Mosca, J.-L. Maurice, J. M. George, A. Fert, and C. Bourgognon, Phys. Rev. B **63**, 094428 (2001).
[11] M. V. Gomoyunova, D. E. Malygin, and I. I. Pronin, Fiz. Tverd. Tela (St. Petersburg) **50**, 1518 (2008) [Phys. Solid State **50**, 1579 (2008)].
[12] K. Paredis, D. Smeets, and A. Vantomme, New J. Phys. **11**, 093019 (2009); Nanoscale Res. Lett. **4**, 1447 (2009).
[13] F. Zavaliche, W. Wulfhekel, H. Xu, and J. Kirschner, J. Appl. Phys. **88**, 5289 (2000).
[14] J. Kudrnovský, N. E. Christensen, and O. K. Andersen, Phys. Rev. B **43**, 5924 (1991).
[15] A. Ionescu, C. A. F. Vaz, T. Trypiniotis, C. M. Gürtler, H. García-Miquel, J. A. C. Bland, M. E. Vickers, R. M. Dalgliesh, S. Langridge, Y. Bugoslavsky, Y. Miyoshi, L. F. Cohen, and K. R. A. Ziebeck, Phys. Rev. B **71**, 094401 (2005).
[16] B. Krumme, C. Weis, H. C. Herper, F. Stromberg, C. Antoniak, A. Warland, E. Schuster, P. Srivastava, M. Walterfang, K. Fauth, J. Minár, H. Ebert, P. Entel, W. Keune, and H. Wende, Phys. Rev. B **80**, 144403 (2009).
[17] G. L. Zhao and M. E. Bachlechner, Phys. Rev. B **58**, 1887 (1998).
[18] Y. Morita and H. Tokumoto, Jpn. J. Appl. Phys. **40**, 4357 (2001).
[19] H. Ahn, C.-L. Wu, S. Gwo, C. M. Wei, and Y. C. Chou, Phys. Rev. Lett. **86**, 2818 (2001); C.-L. Wu, J.-L. Hsieh, H.-D. Hsueh, and S. Gwo, Phys. Rev. B **65**, 045309 (2002).
[20] J. W. Kim and H. W. Yeom, Phys. Rev. B **67**, 035304 (2003).
[21] X. S. Wang, G. Zhai, J. Yang, and N. Cue, Phys. Rev. B **60**, 2146R (1999); G. Zhai, J. Yang, N. Cue, and X. Wang, Thin Solid Films **366**, 121 (2000).
[22] R. M. C. de Almeida and I. J. R. Baumvol, Phys. Rev. B **62**, R16255 (2000).
[23] R. Flammini, R. Belkhou, F. Wiame, S. Iacobucci, and A. Taleb-Ibrahimi, Surf. Sci. **579**, 188 (2005).
[24] H.-M. Lee, C.-T. Kuo, H.-W. Shiu, C.-H. Chen, and S. Gwo, Appl. Phys. Lett. **95**, 222104 (2009).
[25] M. Yang, R. Q. Wu, W. S. Deng, L. Shen, Z. D. Sha, Y. Q. Cai, Y. P. Feng, and S. J. Wang, J. Appl. Phys. **105**, 024108 (2009).
[26] Y. Morita and H. Tokumoto, Surf. Sci. **443**, L1037 (1999).
[27] A. G. Schrott and S. C. Fain Jr., Surf. Sci. **111**, 39 (1981).
[28] M. Nishijima, H. Kobayashi, K. Edamoto, and M. Onchi, Surf. Sci. **137**, 473 (1984).
[29] B. Röttger, R. Kliese, and H. Neddnrmeyer, J. Vac. Sci. Technol. B **14**, 1051 (1996).
[30] E. Bauer, Y. Wei, T. Müller, A. Pavlovska, and I. S. T. Tsong, Phys. Rev. B **51**, 17891 (1995).
[31] K. Edamoto, S. Tanaka, M. Onchi, and M. Nishijima, Surf. Sci. **167**, 285 (1986).

[32]W. Y. Ching, S. D. Mo, and Y. Chen, J. Am. Ceram. Soc. **85**, 11 (2002); W. Y. Ching, L. Ouyang, and J. D. Gale, Phys. Rev. B **61**, 8696 (2000).
[33]G. Dufour, F. Rochet, H. Roulet, and F. Sirotti, Surf. Sci. **304**, 33 (1994).
[34]R. I. G. Uhrberg, G. V. Hansson, J. M. Nicholls, P. E. S. Persson, and S. A. Flodström, Phys. Rev. B **31**, 3805 (1985); R. I. G. Uhrberg, G. V. Hansson, U. O. Karlsson, J. M. Nicholls, P. E. S. Persson, S. A. Flodström, R. Engelhardt, and E.-E. Koch, *ibid*. **31**, 3795 (1985).
[35]T. Nakagawa, Y. Takagi, Y. Matsumoto, and T. Yokoyama, Jpn. J. Appl. Phys. **47**, 2132 (2008).
[36]T. Yokoyama, T. Nakagawa, and Y. Takagi, Int. Rev. Phys. Chem. **27**, 449 (2008).
[37]H. von Känel, K. A. Mäder, E. Müller, N. Onda, and H. Sirringhaus, Phys. Rev. B **45**, 13807 (1992).
[38]S. Walter, F. Blobner, M. Krause, S. Müller, K. Heinz, and U. Starke, J. Phys.: Condens. Matter **15**, 5207 (2003).
[39]A. L. Vazquez deParga, J. de la Figuera, C. Ocal, and R. Miranda, Ultramicroscopy **42–44**, 845 (1992).
[40]W. Raunau, H. Niehus, T. Schilling, and G. Comsa, Surf. Sci. **286**, 203 (1993).
[41]J. Derrien, J. Chevrier, Le Thanh Vinh, I. Berbezier, C. Giannini, S. Lagomarsino, and M. G. Grimaldi, Appl. Surf. Sci. **73**, 90 (1993).
[42]R. Tsushima, Y. Michishita, S. Fujii, H. Okado, K. Umezawa, Y. Maeda, Y. Terai, K. Oura, and M. Katayama, Surf. Sci. **579**, 73 (2005).
[43]A. Wawro, S. Suto, R. Czajka, and A. Kasuya, Phys. Rev. B **67**, 195401 (2003).
[44]F. Sirotti, M. DeSantis, and G. Rossi, Phys. Rev. B **48**, 8299 (1993).
[45]Y. Takagi, K. Isami, I. Yamamoto, T. Nakagawa, and T. Yokoyama, Phys. Rev. B **81**, 035422 (2010).
[46]L. Aballe, L. Gregoratti, A. Barinov, M. Kiskinova, T. Clausen, S. Gangopadhyay, and J. Falta, Appl. Phys. Lett. **84**, 5031 (2004).
[47]J. M. Nicholls and B. Reihl, Phys. Rev. B **36**, 8071 (1987).
[48]B. T. Thole, P. Carra, F. Sette, and G. van der Laan, Phys. Rev. Lett. **68**, 1943 (1992).
[49]P. Carra, B. T. Thole, M. Altarelli, and X. Wang, Phys. Rev.Lett. **70**, 694 (1993).
[50]J. Stöhr and H. König, Phys. Rev. Lett. **75**, 3748 (1995).
[51]C. T. Chen, Y. U. Idzerda, H.-J. Lin, N. V. Smith, G. Meigs, E. Chaban, G. H. Ho, E. Pellegrin, and F. Sette, Phys. Rev. Lett. **75**, 152 (1995).
[52]I. M. L. Billas, A. Châtelain, and W. A. de Heer, J. Magn. Magn. Mater. **168**, 64 (1997).
[53]R. Evans, U. Nowak, F. Dorfbauer, T. Shrefl, O. Mryasov, R. W. Chantrell, and G. Grochola, J. Appl. Phys. **99**, 08G703 (2006).
[54]K. W. Edmonds, C. Binns, S. H. Baker, S. C. Thornton, C. Norris, J. B. Goedkoop, M. Finazzi, and N. B. Brookes, Phys. Rev. B **60**, 472 (1999).
[55]E. E. Carpenter, J. A. Sims, J. A. Wienmann, W. L. Zhou, and C. J. O'Connor, J. Appl. Phys. **87**, 5615 (2000).
[56]J. P. Pierce, M. A. Torija, Z. Gai, J. Shi, T. C. Schulthess, G. A. Farnan, J. F. Wendelken, E. W. Plummer, and J. Shen, Phys. Rev. Lett. **92**, 237201 (2004).
[57]S.-J. Park, S. Kim, S. Lee, Z. G. Khim, K. Char, and T. Hyeon, J. Am. Chem. Soc. **122**, 8581 (2000).
[58]H. Kura, M. Takahashi, and T. Ogawa, J. Phys. D: Appl. Phys. **44**, 022002 (2011).